Simulation of Robotic Friction Stir Welding of Aerospace Components

Antoine Bres[1], Bruno Monsarrat[1,], Laurent Dubourg[1], Lionel Birglen[2], Claude Perron[1] Mohammad Jahazi[1] and Luc Baron[2]*

[1]Aerospace Manufacturing Technology Centre, Institute for Aerospace Research National Research Council Canada, Montreal, Canada

—

[2]Department of Mechanical Engineering, École Polytechnique de Montréal, Montreal, Canada

Abstract

Purpose – The main objective of this work is the establishment of a model-based framework allowing the simulation, analysis and optimization of friction stir welding (FSW) processes of metallic structures using industrial robots, with a particular emphasis on the assembly of aircraft components made of aerospace aluminum alloys.

Design/methodology/approach – After a first part of the work dedicated to the kinetostatic and dynamical identification of the robotic mechanical system, a complete analytical model of the robotized process is developed, incorporating a dynamic model of the industrial robot, a multi-axes macroscopic visco-elastic model of the FSW process and a force/position control unit of the system. These different modules are subsequently implemented in a high fidelity multi-rate dynamical simulation in the MatLAB/Simulink environment.

Findings – The developed simulation infrastructure allowed the research team to analyze and understand the dynamic interaction between the industrial robot mechanics, the control architecture and the manufacturing process involving heavy load cases in different process configurations. Several critical process-induced perturbations such as tool oscillations and lateral / rotational deviations were observed, analyzed and quantified during the simulated robotic friction stir welding operations.

Practical implications – The presented simulation platform will constitute one of the key technology enablers in the major research initiative carried out by NRC Aerospace in their endeavor to develop a robust robotic FSW platform, allowing both the development of optimal workcell layouts / process parameters and the validation of advanced real-time control laws for robust handling of critical process-induced perturbations. These deliverables will be incorporated in the resulting robotic FSW technology packaged for deployment in production environments.

Originality/value – This work establishes the first model-based framework allowing the high fidelity simulation, analysis and optimization of friction stir welding processes using serial industrial robots.

Keywords Friction stir welding, industrial robot, aerospace component assembly, multi-rate dynamical simulation

Paper type Research paper

1. Introduction

Friction stir welding (FSW) is an emerging manufacturing technology for aerospace structures. It will see widespread use in the future as it offers ways of creating lighter structures at lower manufacturing cost than traditional methods (riveting, adhesive bonding). Since its invention in 1991, FSW has known fast improvements and many studies have demonstrated its capability for joining a wide range of materials [1]-[5]. As shown in Figure 1, the process involves a rotating tool consisting of a pin and a shoulder. The pin is inserted between adjoining metal pieces and the shoulder remains at the top surface of the joint. The heat generated by the tool friction brings the metal to a plastic-like state and the pin mixes together the metal in the joint area resulting in a sound and homogenous joint. Unlike traditional welding processes (laser welding, GTAW, GMAW), the melting point of the materials to be joined is not reached during FSW operation, reducing the probability of distortions, porosities and loss of mechanical properties. Moreover, the technology can join heat treatable aluminum alloys, for example 2XXX

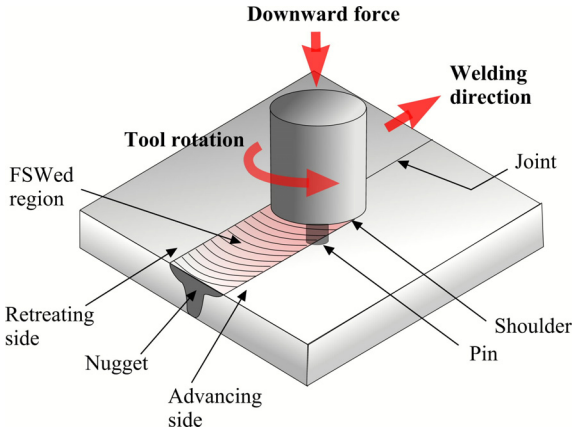

Figure 1 Schematic description of the friction stir welding process. The weld is realized by a combined advance and rotation of the tool without any addition of material, enabled by the control of the depth force, tool spindle speed and advance and transversal position & orientation of the tool.

*All correspondence related to this manuscript should be directed to corresponding author (e-mail: Bruno.Monsarrat@cnrc-nrc.gc.ca, Phone : +1-514-283-9259, Docufax: +1-514-283-9604)

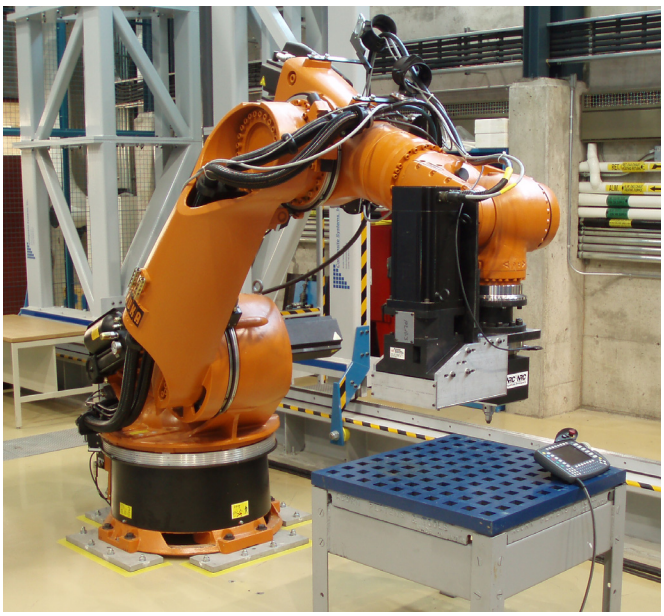

Figure 2 Robotic friction stir welding test-bed located at the NRC Aerospace Manufacturing Technology Centre incorporating modified high payload KUKA KR500 MT industrial robot and commercial electrically-driven process end-effector. The system is used as hardware development platform as well as demonstrator for NRC developed technology packages.

and 7XXX series, many of which are considered difficult to weld using traditional processes [6-12]. The relative high welding speed and repeatability, no filler and no preparation, improved mechanical properties and low residual stresses make of FSW a beneficial manufacturing method for marine, railways, construction and aerospace industries. Although the presented work can be applied to any of the aforementioned industries, the present paper will focus on aircraft assembly operations.

More specifically, aircraft fuselage panels are typically composed of stringers and frames assembled to a skin using one or two-piece mechanical fasteners. Both drilling and countersinking operations followed by the application of a sealant are generally required prior to the installation of each fastener. Because its use results in reducing the weight of the aircraft, shortening the process cycle time, reducing the cost of assembly operations and simultaneously generating a smooth aerodynamic profile [5,15], the FSW process [Figure 3(a)] represents an excellent alternative to fasteners for assembling large aerospace structures [13],[14].

The Institute for Aerospace Research of the National Research Council Canada (NRC Aerospace) undertook a major initiative to manufacture large scale representative aircraft structural elements, such as fuselage panels, using FSW. This multi-pronged study includes the aspects of structural design, process optimization, mechanical properties, NDE and robotic processing. Specific emphasis is given in the present paper on works performed at the NRC Aerospace Manufacturing technology Centre (AMTC) to develop a specialized robotic FSW technology ready for deployment in production environments for the assembly of aeronautic components. At the end of the project, it is intended to demonstrate the assembly of large scale representative candidate structural elements using the specialized test-bed implemented in its Montreal facility, as shown in Figure 2.

1.1 Main challenges in stringer to skin friction stir welding of aeronautic components

Despite the numerous advantages presented in the previous subsection, skin to stringer joints still pose significant problems for FSW because of the defects associated with manufacturing FSW lap welds, such as hooking, kissing bonds, top plate thinning and voids. Some of these problems can be alleviated by modifying welding parameters including pin geometry, number of weld passes, rotation direction, etc.

In a recent study [31], NRC researchers investigated the effects of process parameters on weld quality of 1,5-mm 7075-T6 stringers lap-joined on 2,3-mm 2024-T3 skins. Advancing and retreating side locations on the joint configuration were alternated to determine optimal design arrangement. Different FSW tool geometries, such as smooth, threaded, pyramidal and truncated pins, were used to evaluate the impact of the tool shape on the weld quality, i.e. the presence of hooking, kissing bond or voids. Moreover, the effects of pin length, roll angle, forge force, welding and rotation speeds on weld quality and defect generation were also investigated. Weld quality was assessed by optical microscopy and bending tests. Significant mechanical testing, metallography and fractography were used to compare different coupon configurations, specifically in terms of the fatigue properties. Moreover, different weld configurations were manufactured: discontinuous (with plunge-in entry and exit holes), continuous welds, single pass welds, double pass welds, and plugged discontinuous welds. The results are also compared with riveted lap joint of identical geometry mainly in terms of cyclic strength performance of FSW panels. In this study, typical load cases required to achieve high performance FSWelded stringer to skin lap joints were determined using the *MTS-ISTIR* FSW machine [16] located in the AMTC facility. Strength up to 18kN was reported in depth direction and up to 4kN and 1kN in respectively longitudinal and transversal directions. The reader is referred to as Figure 3(b) for the detailed force data readings. It was also observed that, due to the geometry of the tool and its imperfections, the process forces are not constant during a rotation of the spindle, resulting in a variation of the forces whose frequency is linked to the spindle speed.

1.2 Robotic friction stir welding: state-of-the-art

To the best knowledge of the authors, all FSW systems currently in production to manufacture aerospace components use gantry-type CNC systems. Representative applications are the replacement of rivets in the stiffener to skin assembly on NASA's launch vehicle dry bay structures [23] or the certified *Eclipse 500* business jet where 60 % of all rivets have been replaced by 136m of FSWelded lap joints [24].

These recent years, an effort has been made to democratize FSW by replacing dedicated CNC machines by more versatile industrial robots. The use of industrial robots with parallel kinematics has been investigated and their feasibility for welding 3-dimensional profiles was demonstrated by a research team at the GKSS research centre [25]. Despite good

accuracy, stiffness and payload performance, the latter, however, exhibit limited work envelopes and orientation capabilities for a remaining prohibitive acquisition cost.

On the other hand, heavy payload serial industrial robots are far less bulky, exhibit a larger workspace for a fraction of the acquisition cost. Several initiatives can be reported in the field in FSW process industrialization using serial robots. A team from Örebro University, Sweden, investigated the use of position / force control to achieve FSW on an ABB IRB 7600-500 industrial robot, whose last link was directly replaced by the process end-effector [26]. Such an arrangement was chosen to reduce the torques exerted on the two remaining joints of the spherical wrist, the latter been those with higher compliance. Another FSW system is based upon use of the same industrial robot platform, with published applications reporting welding of 6XXX series aluminum alloys with thicknesses up to 25 mm [27]. A major initiative was also carried out by the EADS Corporate Research Centre in Munich, Germany, to industrialize the FSW process in commercial aircraft component assembly applications [17]. In the latter case, a KUKA KR500 serial industrial robot was modified heavily for the task at hand, with a substantial payload increase allowing the system to achieve process forces of up the 10kN, thus enabling the robot to weld aerospace aluminum sections of more than 5mm. The capabilities of this state-of-the-art industrial platform motivated NRC Aerospace researchers to integrate this industrial robot as part of their robotic FSW infrastructure, as depicted in Figure 2.

1.3 Limitations associated with existing technology incorporating serial industrial robots

In the aforementioned references, two types of limitations associated with FSW process automation using industrial serial robots can be highlighted. The first pertains to the inherent payload capability limit that is highly dependent on the robot configuration. It was shown in these works that proper design of the workcell layout and / or reduction of the FSW tool pin diameter—reducing the required process induced forces—can open a certain feasibility window in terms of payload capability in a generally small but sufficient subspace of the robot work envelope. The second limitation pertains to the perturbations induced during the process by the important elasticity of the joints in serial industrial robots. As a matter of fact, both lateral deviations—typically of several millimeters amplitude— and loss of normality of the tool are caused by the deformation of the robot joints under the high process-induced forces, such physical effects having great influence on the weld quality [18]. Considering that, for a butt joint, the weld quality is only preserved as long as the center of the FSW tool does not have a transversal deviation superior to half the diameter of the tool pin [19], tool deviations have the potential to severely impact the resulting weld quality.

Although imposing strong limitations and affecting the level of flexibility of the resulting technology, these issues were managed empirically in the aforementioned initiatives involving industrial serial robots. A representative example of that is that the lateral tool deviations, when addressed, were measured in sample welding configurations before being integrated manually in robot trajectories, with varying reported results in the different publications depending on the trajectory profiles and part geometry.

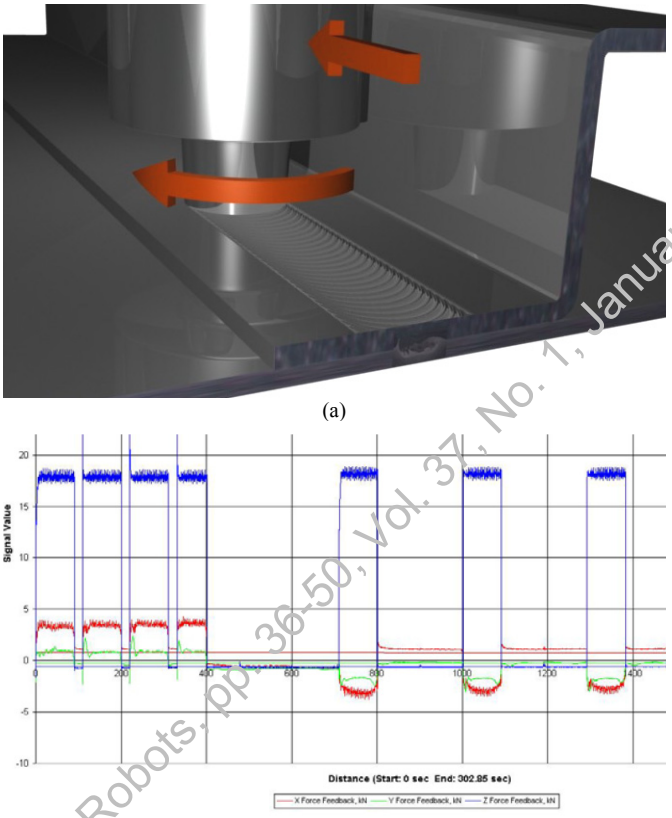

(a)

(b)

Figure 3 (a) Digital illustration of friction stir welding of a stringer to skin lap joint on a typical aerospace component and (b) amplitude of the forces at the tip of the FSW tool during a test on the NRC Aerospace *MTS-ISTIR* welding machine.

Based on these observations, it becomes obvious that the implementation of FSW process using industrial robot is a difficult task due to the important lack of scientific formalism in the modeling, analysis, simulation and optimization of robotic friction stir welding, whatever it is gantry-type, parallel or serial kinematics used as motion system. Such a framework would allow designers to use a formal methodology to synthesize optimal workcell layouts and process parameters taking full advantage of the selected motion system. In addition, a model-based formalism opens avenues to design and validate advanced real-time control laws for robust handling of critical process-induced perturbations, including those associated with the joint compliances.

1.4 Objectives of presented study

The main objective of this work is the establishment of a technological framework allowing the simulation, analysis and optimization of friction stir welding processes of metallic structures using industrial robots, with a particular emphasis on the assembly of aircraft components made of aerospace aluminum alloys. The developed models will be incorporated in a high fidelity simulation platform developed to provide NRC Aerospace researchers with new capabilities to design

robotic FSW applications, including:

- In-depth study of the dynamical interaction between the industrial robot mechanics, the control architecture and the heavy process-induced load cases;
- Determination of the optimal workcell layout for a family of aircraft components;
- Synthesis of the maximum robotic process parameters (payload, tool design, rotation / advance parameters, etc);
- Sensitivity analysis against critical process parameters;
- Implementation / validation of advanced control laws allowing the industrialization of the process with robust handling of all process-induced perturbations.

1.5 Organization of present paper

After a first part of the work dedicated to the kinetostatic and dynamical identification of the robotic mechanical system presented in Section 2, a complete analytical model of the robotized process is developed in Section 3, incorporating a dynamical model of the serial industrial robot, a multi-axes macroscopic visco-elastic model of the friction stir welding process and a force/position control unit of the system. These different modules are subsequently implemented in a high fidelity multi-rate simulation in the MatLAB/Simulink environment, as discussed in Section 4. Simulation results in the context of the robotic friction stir lap welding of stringers on a 2024-T3 aircraft component skin are finally presented and discussed in the last part of the paper. The authors will conclude will some remarks about the opportunities offered by the new simulation platform and the ongoing/future work carried out by the research team.

2. Identification of relevant plant parameters

As mentioned in the introduction, NRC Aerospace FSW test-bed incorporates a high payload KUKA KR 500 MT industrial robot. This robot is a heavily modified version of the commercial off-the-shelf KR500 robot equipped with different gearboxes on the three first axes with transmissions ratios having twice the amplitudes of that of the standard KR500 version. Such a modification doubles the maximum torque capability of the first three motors with the counterpart that the maximal angular velocities are reduced by the same factor. The motors also received some modifications that are not detailed here because they do not drastically impact their characteristics. In addition, the three axes of the spherical wrist are identical to the original version. Consequently, the increase of the payload capability is mainly in an axis passing through the center of the robot spherical wrist, which is very adequate to most FSW end-effector arrangements reported in the literature where the main process force axis does only solicitate the first three motors. In order to develop a simulation of the robotized FSW process, the first task was to develop geometric, kinematic and dynamical models of the KR500 MT robot, requiring accurate model parameters.

To achieve this task, the geometric parameters of the robot, in the form of its Denavit-Hartenberg parameter matrix [30], were collected using data directly accessible in robot configuration files. Also, confidential parameters describing the robot dynamics, i.e., link mass and inertial parameters, gear ratios, inertias of drive units and data of spring compensation system were kindly provided to the research team by the robot manufacturer. Two classes of kinetostatic and dynamic parameters, i.e., the robot *real* joint elasticities and damping factors, remained inaccessible but mandatory for the sake of accurate robot forward dynamics implementation. In this context, specific identification procedures were implemented for the estimation of these parameters on the physical system, as described hereafter.

2.1 Kinetostatic identification of the industrial robot

The present section pertains to the identification of those parameters stemming from the structural deformation of the robot links and joints due to the application of external loads. Such errors are typically associated with individual links flexibility, actuators elasticity and gear backlash. It is typically admitted in all significant works in the field of industrial robot calibration, however, that in the case of the type of industrial robots under study, (i) the links are designed with high stiffness, and (ii) most of the structural deformation due to articular elasticity is from far the most significant positional inaccuracies contributor [28],[29]. For this reason, the assumption was made by the authors to develop a kinetostatic model of the KR500 MT robot incorporating only those effects induced by articular elasticities, each of these being modeled as a linear torsional spring acting about its associated joint axis.

In order to minimize the logistics for parameters estimation, it was decided to take profit of the gravity compensation module integrated in the KR500 MT control unit. The implemented algorithms use an elastostatic model of the robot, when manipulating a known payload, to estimate the deflection of the tool-center-point (TCP) subject to gravitational effects. Using this module, trajectories can be corrected accordingly online to compensate for the resulting errors using a *fake target* approach (see Figure 4).

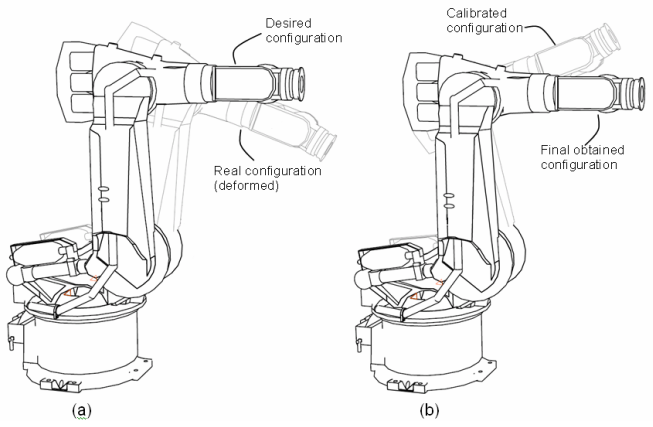

Figure 4 Gravity compensation principle: (a) illustration of the positional error due to joint deformations under the load and (b) calibrated command sent to the actuators to compensate the deformation with illustration of the obtained robot configuration.

Let $\Delta\boldsymbol{\theta}$ be the articular correction vector applied by the robot controller to compensate for the deformation induced by a load of mass m and $\boldsymbol{\tau}$ the vector of actuator torques required to maintain the robot configuration, one has the relation:

$$\boldsymbol{\tau} = \mathbf{K}_{\theta}\Delta\boldsymbol{\theta} \tag{1.1}$$

where $\mathbf{K}_{\theta}$ is the 6x6 diagonal matrix of the six articular stiffnesses. The torque vector $\boldsymbol{\tau}$ appearing in equation (1.1) is computed with the well known static relation [20]:

$$\boldsymbol{\tau} = \mathbf{J}^{T}\mathbf{w}\ , \qquad \text{with}\ \ \mathbf{w} \equiv \begin{bmatrix} \mathbf{c}\times m\mathbf{g} \\ m\mathbf{g} \end{bmatrix} \tag{1.2}$$

where $\mathbf{w}$ is the external wrench applied on the robot flange, $\mathbf{c}$ is the center of mass (com) location, $\mathbf{g}$ the gravitational vector and $\mathbf{J}$ is the Jacobian matrix mapping the robot articular velocities into the associated Cartesian twist. In the field of small displacements, a 1st order approximation of the robot instantaneous kinematics can be formulated in the form:

$$\Delta\mathbf{x} \simeq \mathbf{J}\Delta\boldsymbol{\theta}\ , \qquad \text{with}\ \Delta\mathbf{x} \equiv \begin{bmatrix} \mathbf{vect}(\Delta\mathbf{Q}\mathbf{Q}^{\mathrm{T}}) \\ \Delta\mathbf{p} \end{bmatrix} \tag{1.3}$$

with $\mathbf{p}$ and $\mathbf{Q}$ being the tool center position vector and the orientation matrix, respectively and $\mathbf{vect}(\cdot)$ being the vector linear invariant of its matrix argument. Substituting Eqs. (1.2) and (1.3) into Eq. (1.1), one obtain, for nonsingular robot configurations, a relation between the Cartesian error vector $\Delta\mathbf{x}$ and the external wrench due to gravitational effects :

$$\mathbf{w} = \mathbf{K}_{c}\Delta\mathbf{x} \tag{1.4}$$

with $\mathbf{K}_{c} = \mathbf{J}^{-T}\mathbf{K}_{\theta}\mathbf{J}^{-1}$ being the equivalent 6x6 Cartesian stiffness matrix. Using this relation, our identification protocol for the identification of the elasticities of axes 2 to 6 could be formulated. In fact, we modified the load definition parameters in the robot controller configuration files from 0 to 500 kg and measured the Cartesian correction along trajectories chosen for their ability to excite, with sufficient torque levels, a given subset of the robot joints. In order to get the end-effector position and orientation in each configuration, a multifunction end-effector was instrumented with 3 optical reflectors whose locations were previously calibrated in the flange frame using a geometric protocol. For each configuration, the associated external wrench $\mathbf{w}$ induced by the load increase was computed and the induced Cartesian error vector $\Delta\mathbf{x}$ was determined using metrology measurements. Joints elasticities were finally calculated from Eq. (1.4). The instrumentation of the robotic test-bed and some sample results are provided in Figure 5(a).

Because the 1st joint axis is collinear to the gravity direction, another protocol was used to identify its elasticity. In fact, as depicted in Figure 5(b), the robot was put in contact with a rigid tooling before initiating a small displacement in the contact direction. The induced load case was measured using a force sensor, allowing direct calculation of the joint elasticity.

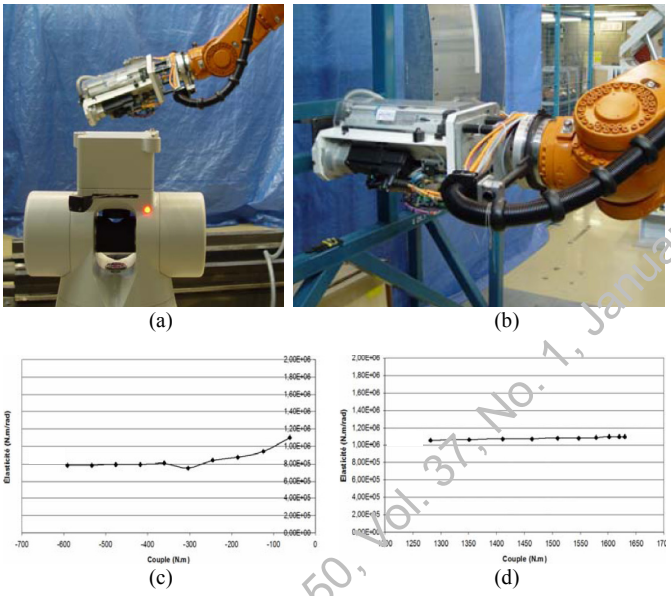

Figure 5 (a) The multi-function end effector (for drilling/countersinking, and fastener installation) mounted on the KR500 MT is equipped with the optical reflectors to capture the position and orientation of the flange with a laser tracker metrology system. (b) Illustration of the protocol used to identify the stiffness of the first joint in contact on a rigid tooling. (c,d) estimated elasticities for axes 4 and 5 as a function of the applied torques.

2.2 Identification of dynamical parameters of KR500 MT industrial robot

As discussed previously, most dynamical parameters were obtained from the robot manufacturer. We needed, however, in order to develop an accurate robot dynamics, to identify the joint damping factors. The procedure implemented for the estimation of these parameters on the physical system is described in the present subsection.

In fact, it appeared to the authors that the easiest way to identify the damping of the joints was to initiate a movement on the desired joint and then stop it abruptly using the built-in brakes of the robot. The implied vibrations were then captured at 1000Hz using a laser tracker metrology system measuring an optical reflector located on the link following immediately the joint of interest, as shown in Figure 6. We had to consider the fact that a stimulation of a given joint also induces vibrations on some of the remaining joints, depending on the robot posture and coupling of inertial effects. To circumvent this problem, specific robot postures were found that isolated the other joints from the influence of the commanded motion. In more complex cases, as for example joints 2 and 3 with collinear axes, the measured dynamic response are highly coupled. However, because parameters such as link masses, inertias and joint elasticities are known, eigenfrequencies associated with each joint response can be computed and the signals measured by the metrology system can be separated with adequate filtering. Once the oscillations of the different joints were isolated, the response of a classic second order oscillating system with damping could be observed. The robot configuration used and the filtered response in the case of the

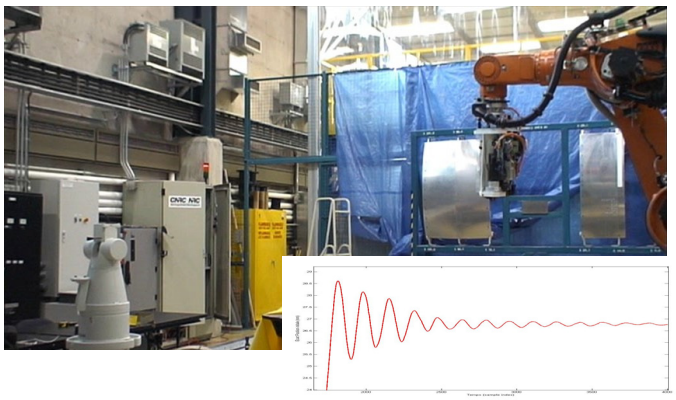

Figure 6 Setup used to identify the damping of the joints with a laser tracker metrology system capturing the position of an optical reflector located on the end effector at a 1000Hz frequency. The illustrated robot configuration was used for the identification of the joint 4. In the bottom right corner, the filtered result of the measurements.

identification of the robot 4th joint are shown in Figure 6 to illustrate the procedure. For each of the 6 filtered responses, the damping factor was determined with the relation:

$$c = \frac{2}{T}\ln\left(\frac{A_1}{A_2}\right) \tag{1.5}$$

where c is the identified articular damping factor, T is the period of the oscillations, and A_1 and A_2 are the amplitudes of two successive oscillations.

2.3 Identification of a force process model

In order to predict the mechanical interaction between the robot mechanics, position/control scheme and FSWelded material, a model of the FSW process was needed for the sake of high fidelity RFSW simulation, involving calculation steps of 1ms or less, and eventually subsequent real-time controller implementation. Those available in the literature relied vastly on numerical techniques, involving either solid or fluid mechanics approaches [32]. Although leading to good correlation with experimental data, such numerical models were computationally intensive and not adapted for high frequency RFSW simulation or control purposes.

On the other hand, only very few works reported the development of macroscopic FSW process models ready for soft or hard real-time computations. To the best knowledge of the authors, none were available in published literature during the developments of the NRC team. Only in a recent publication [33], a one-dimensional FSW model was proposed allowing a computationally efficient calculation of the normal force as a nonlinear function of the measured FSW process parameters in both static and dynamic regimes. The model was implemented in a nonlinear feedback controller for the axial force. In parallel to this development, the authors developed, during the first semester 2007, a 3-dimensional visco-elastic model explicit in terms of the FSW tool position and velocity vectors. The model was validated with excellent correlation using experiments lead on NRC *MTS-ISTIR* system. The model also includes a dynamic perturbation simulating the force variations induced by the tool rotation.

3. Model Development for robotic FSW process

In this section, we present the model-based framework that was developed by the authors for the accurate simulation of friction stir welding processes of metallic structures using serial industrial robots. In addition to the motion control laws and process model, the developed analytical framework incorporates the following modules for the modeling of the KR500 MT industrial robot mechanics:

- F*orward kinematics* module mapping the joint position and velocity vectors $\boldsymbol{\theta}$, $\dot{\boldsymbol{\theta}}$ into the Cartesian position vector $\mathbf{p}$, orientation matrix $\mathbf{Q}$ and Cartesian twist vector $\mathbf{t} = [\omega^T \quad \dot{\mathbf{p}}^T]^T$, where ω is the Cartesian angular velocity vector.
- *Inverse kinematics* realizing the inverse mapping of the one achieved by the previous module.
- *Forward dynamics* module for calculation of robot joint-variable time-histories $\boldsymbol{\theta}(t)$ as a function of articular forces/torques and external wrench.

The reader is referred to as reference [20] for information about the forward and inverse kinematics modeling techniques for serial decoupled manipulators. The forward dynamics module and motion control laws are discussed with more details in the following subsections.

3.1 High fidelity dynamical model of KUKA KR500 MT industrial robot

The developed dynamic model of the KR500 MT industrial robot integrates both link and actuators dynamics in addition to joint elasticities and damping factors as identified in subsections 2.1 and 2.2, respectively. Based on a given articular torque vector $\boldsymbol{\tau}$ and external wrench $\mathbf{w}$, and because it integrates joint structural behavior, the forward dynamics had to be simultaneously solved for the robot joint-variable time-histories in terms of both the vector of encoder-read values $\boldsymbol{\theta}_E(t)$ and the vector of *real* joint positions $\boldsymbol{\theta}(t)$, the latter representing the actual physical configuration of the robot. These two articular vectors being linked by the articular stiffness matrix $\mathbf{K}_\theta$ and diagonal matrix of damping ratios $\mathbf{D}_\theta$, the forward dynamical equations of the industrial robot were formulated in the form of the following system of coupled this differential equations [21]:

$$\begin{cases} \mathbf{I}\ddot{\boldsymbol{\theta}} + \mathbf{C}\left(\dot{\boldsymbol{\theta}}, \boldsymbol{\theta}\right) + \mathbf{D}_\theta\left(\dot{\boldsymbol{\theta}} - \dot{\boldsymbol{\theta}}_\mathbf{E}\right) + \mathbf{K}_\theta\left(\boldsymbol{\theta} - \boldsymbol{\theta}_\mathbf{E}\right) = \mathbf{0} \\ \mathbf{I}_\mathbf{M}\ddot{\boldsymbol{\theta}}_\mathbf{E} - \mathbf{D}_\theta\left(\dot{\boldsymbol{\theta}} - \dot{\boldsymbol{\theta}}_\mathbf{E}\right) - \mathbf{K}_\theta\left(\boldsymbol{\theta} - \boldsymbol{\theta}_\mathbf{E}\right) = \boldsymbol{\Gamma} \end{cases} \tag{2.1}$$

where $\mathbf{I}$ and $\mathbf{I}_\mathbf{M}$ are respectively the generalized inertia matrix, incorporating the link inertial parameters, and the inertia matrix of the joint motors / gearboxes in the space of the robot articulations. $\boldsymbol{\Gamma}$ represents the vector of the actuator torques. In addition, $\mathbf{C}$ is the vector of the torques induced by all the kinetic effects during robot motion.

In practice, the forward dynamics, i.e. the computation of state vectors associated with joint-variables $\boldsymbol{\theta}_E(t)$ and $\boldsymbol{\theta}(t)$

from Eq. (2.1), is achieved as follows. The first step consists in calculating the term $\mathbf{C}(\dot{\boldsymbol{\theta}},\boldsymbol{\theta})$ representing the articular torque required to produce the motion in the absence of dissipative wrenches and joint accelerations. It is efficiently computed using a recursive inverse dynamics algorithm, as for instance the one provided in [20], in the special case of $\ddot{\boldsymbol{\theta}} = \mathbf{0}$ in presence of both gravitational effects and external non-dissipative wrench. All terms appearing in Eq. (2.1) depending on coordinates $\boldsymbol{\theta}$, $\boldsymbol{\theta}_{\mathbf{E}}$ and velocities $\dot{\boldsymbol{\theta}}$, $\dot{\boldsymbol{\theta}}_{\mathbf{E}}$ are also evaluated for the current simulation time. In the next step, generalized inertia matrix $\mathbf{I}$, due to its symmetric positive definite nature, can be inverted efficiently using a Cholesky resolution. The inversion of the diagonal inertia matrix $\mathbf{I}_{\mathbf{M}}$ is straightforward. Finally, encoder and real joint coordinate vectors $\boldsymbol{\theta}_{\mathbf{E}}$ and $\boldsymbol{\theta}$ are evaluated independently for the next simulation time step using a proper integration scheme.

3.2 Candidate control structures for process robotization

It is now well established that the physical implementation of robotic FSW requires the use of force control in the depth direction, the complementary directions involving standard position control schemes [32]. In order to stabilize and accurately control the motion of the KR500 MT robot during a simulated FSW operation, a force control scheme needed to be incorporated in the simulation environment. Although a specialized nonlinear control scheme was developed by the authors in [33] with the argument that a stability problem could occur during the initial phase of a robotic FSW operation, other published references presenting applications of FSW using serial industrial robot, i.e., [17],[26],[27], all report efficient and stable force control in the welding depth direction using linear control schemes.

Based on these reported successful implementations and the fact that a nonlinear control scheme is dependent on a window of process parameters requiring implementation of an identification protocol, the authors decided to select a suitable control approach among three different linear control structures evaluated in simulation. In all cases, the industrial robot was driven under hybrid linear force / position control using both positional and force sensor data. As shown in Figs 7, 8 and 9, the common denominator of the 3 controller implementations is in that the encoder reading were simulated using the forward dynamics calculated encoders variables $\boldsymbol{\theta}_{\mathbf{E}}$ while the force sensor data readings were emulated using the process model with inputted *real* joint coordinates $\boldsymbol{\theta}$. The 3 evaluated control schemes are detailed hereafter.

A first structure known as force/position hybrid control with sum of the articular torques was implemented in the simulation infrastructure, as shown in Figure 7. It is based on a parallel resolution of the computed torques in a way that the directions under position control are completely decoupled to those controlled in force in the operational space.

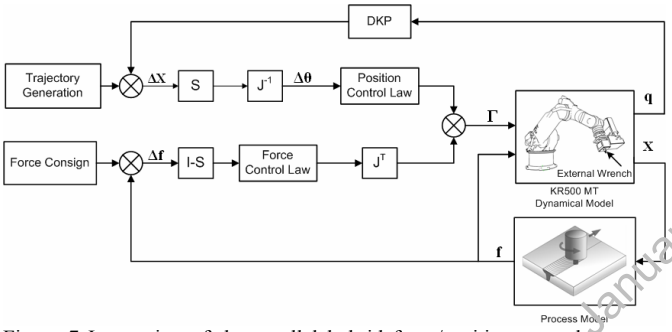

Figure 7 Integration of the parallel hybrid force/position control structure with purely force controlled tool depth.

Complementary selection matrixes are used to assure that the corrections are independent in the operational space. The actuator torque vector is calculated as follows:

$$\boldsymbol{\Gamma} = \mathbf{S}\left[\mathbf{K}_{\mathbf{p}}\mathbf{J}^{-1}\Delta\mathbf{X} + \mathbf{K}_{\mathbf{d}}\frac{d}{dt}\left[\mathbf{J}^{-1}\Delta\mathbf{X}\right] + \mathbf{K}_{\mathbf{i}}\int_{t_0}^{t}\mathbf{J}^{-1}\Delta\mathbf{X}d\tau\right] + \left(\mathbf{I}-\mathbf{S}\right)\mathbf{J}^{\mathbf{T}}\left[\mathbf{f}_{\mathbf{d}} + \mathbf{K}_{\mathbf{pf}}\Delta\mathbf{f} + \mathbf{K}_{\mathbf{df}}\dot{\mathbf{X}} + \mathbf{K}_{\mathbf{if}}\int_{t_0}^{t}\Delta\mathbf{f}d\tau\right] \quad (2.2)$$

where a linear PID control law was used for the force feedback loop with the difference that the derivative term is applied to the Cartesian velocity in the weld depth direction instead of the force derivative associated with noisy sensor readings. Because the encoder signal is the only available from the robot controller, the Cartesian velocity vector is computed from the derivative of the encoder joint variable $\dot{\boldsymbol{\theta}}_{\mathbf{E}}$ using the forward kinematics. Also, the desired force vector is summed to the other PID terms to generate, in static mode, torques of sufficient amplitude to compensate the force command. The remaining directions are position-controlled.

The second evaluated structure is very close to the precedent, as depicted in Figure 8, the only difference being the absence of selection matrix in the position feedback loop. The consequence of such a structure is that the depth of the FSW tool is then controlled simultaneously in position and in force. The desired priority on one of the control types is managed by the control designer with a suitable modulation of the gains of the integrators in the integrator plus derivative structures of the position and force feedback loops.

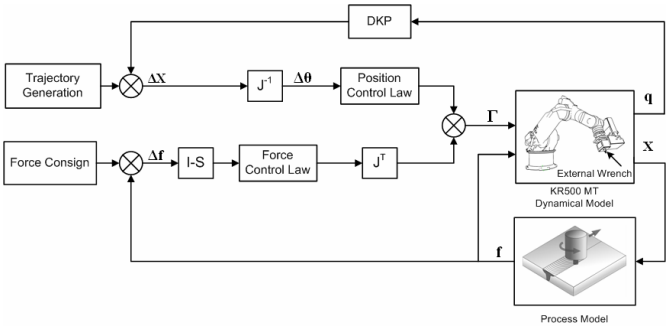

Figure 8 Implementation of the partially decoupled hybrid force/position control structure with superposed control in the tool depth direction.

For this second approach, the torque values sent to actuators are calculated as follows:

$$\boldsymbol{\Gamma} = \mathbf{K}_\mathbf{p}\mathbf{J}^{-1}\Delta\mathbf{X} + \mathbf{K}_\mathbf{d}\frac{d}{dt}\left[\mathbf{J}^{-1}\Delta\mathbf{X}\right] + \mathbf{K}_\mathbf{i}\int_{t_0}^{t}\mathbf{J}^{-1}\Delta\mathbf{X}d\tau + \left(\mathbf{I}-\mathbf{S}\right)\mathbf{J}^{\mathrm{T}}\left[\mathbf{f}_\mathbf{d} + \mathbf{K}_\mathbf{pf}\Delta\mathbf{f} + \mathbf{K}_\mathbf{df}\dot{\mathbf{X}} + \mathbf{K}_\mathbf{if}\int_{t_0}^{t}\Delta\mathbf{f}d\tau\right] \quad (2.3)$$

The 3rd studied control structure is presented in Figure 9. It is characterized by the presence of two imbricated control loops: an external loop corresponding to a force control and the internal loop corresponding to the industrial robot articular motion control. The output of the external force control loop is transformed into a position command through an equivalent environmental stiffness matrix. In the more specific context of our robotic FSW application, the normal force error is transformed into an additional depth correction via an estimated stiffness of the process. The advantage of this last control scheme is that it can be implemented in an existing industrial robot controller without modification of the original articular position control structure.

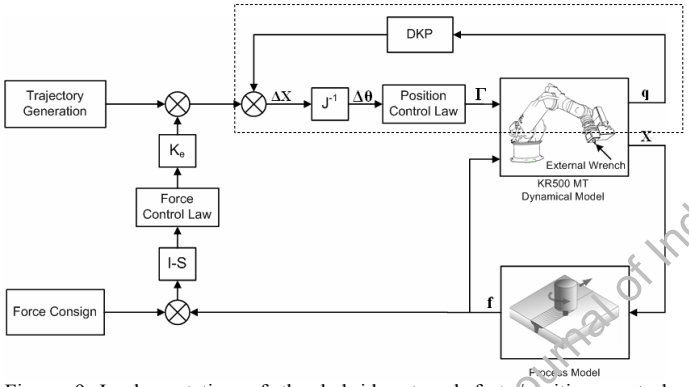

Figure 9 Implementation of the hybrid external force/position control structure with cascaded control loops in the tool depth direction. The position control loop in the dashed area replicates the original control scheme available in the KR500 MT industrial control cabinet.

For this last control structure, the articular torque vector is computed using the following control law:

$$\boldsymbol{\Gamma} = \mathbf{K}_\mathbf{p}\mathbf{J}^{-1}\left(\Delta\mathbf{X} + \Delta\mathbf{X}_\mathbf{f}\right) + \mathbf{K}_\mathbf{d}\frac{d}{dt}\left[\mathbf{J}^{-1}\left(\Delta\mathbf{X} + \Delta\mathbf{X}_\mathbf{f}\right)\right] + \mathbf{K}_\mathbf{i}\int_{t_0}^{t}\mathbf{J}^{-1}\left(\Delta\mathbf{X} + \Delta\mathbf{X}_\mathbf{f}\right)d\tau \quad (2.4)$$

where the additional depth correction is given by :

$$\Delta\mathbf{X}_\mathbf{f} = \mathbf{K}_e\left(\mathbf{I}-\mathbf{S}\right)\mathbf{J}^{\mathrm{T}}\left[\mathbf{f}_\mathbf{d} + \mathbf{K}_\mathbf{pf}\Delta\mathbf{f} + \mathbf{K}_\mathbf{df}\dot{\mathbf{X}} + \mathbf{K}_\mathbf{if}\int_{t_0}^{t}\Delta\mathbf{f}d\tau\right] \quad (2.5)$$

with $\mathbf{K}_e$ being the estimated stiffness matrix. The force error is computed in this last case using the exact same formulation as for the two other evaluated control schemes.

4. Implementation of multi-rate dynamical simulation of robotic FSW process

The different models presented in the previous section were then implemented in the MatLAB/Simulink environment [22]. The following subsections describe the methodology used to implement, validate and then combine the models of the serial industrial robot, FSW process and linear control.

4.1 Integration of KR500 MT forward dynamics

The implementation of the robot forward dynamics was performed in two steps to ensure the consistency and accuracy of the algorithms. First, a partial model incorporating the link and motors dynamics, but with rigid joint behavior was implemented in the MatLAB/Simulink environment. The model was validated when executing several trajectories in free motion mode (without contact of the end-effector with the environment). More specifically, the computed joint motion was compared to the one simulated using an equivalent numerical model of the KR500 MT industrial robot developed using the MatLAB/SimMechanics toolbox [34]. Excellent correlation of results allowed the certification of a substantial part of the direct and forward kinematics modules in addition to the forward dynamics module, including kinetic terms and generalized inertia matrix computations, Cholesky solver for matrix inversion and selected continuous-time integration scheme.

In the second part of the implementation, estimated real elasticities and damping of the robot joints were incorporated according to the formalism and resolution approach described in Subsection 3.1. As depicted in Figure 10, the forward dynamics block receives two inputs: 1–the torque vector computed by the control unit, running at 83Hz, transformed into a high frequency signal (≥1000Hz) using a rate transition block operating a nondeterministic transfer of data with minimum latency, and 2–the external wrench containing the Cartesian normal and lateral forces induced by the FSW process, and computed with the same time step as the forward dynamics. The block outputs both the encoder and real joint-variables $\boldsymbol{\theta}, \boldsymbol{\theta}_\mathbf{E}$ in addition to their respective Cartesian vector counterparts calculated using the robotic manipulator forward kinematics.

4.2 Implementation of FSW force process model

The FSW force process model was integrated in the MatLAB/Simulink environment in parallel to the complete robot forward dynamics. The block computes, for given process parameters, FSW tool position and velocity, the external reaction force induced by the process on the distal link of the robot. The inputted Cartesian position is the one computed in the forward dynamics module based on the *real* joint-variables vector $\boldsymbol{\theta}$. The outputted vector is the process-induced wrench that is used as input of both the manipulator forward dynamics block and the force control unit where this signal replicates the reading of the 6-degree-of-freedom ATI Omega 190 force sensor mounted on the process end-effector.

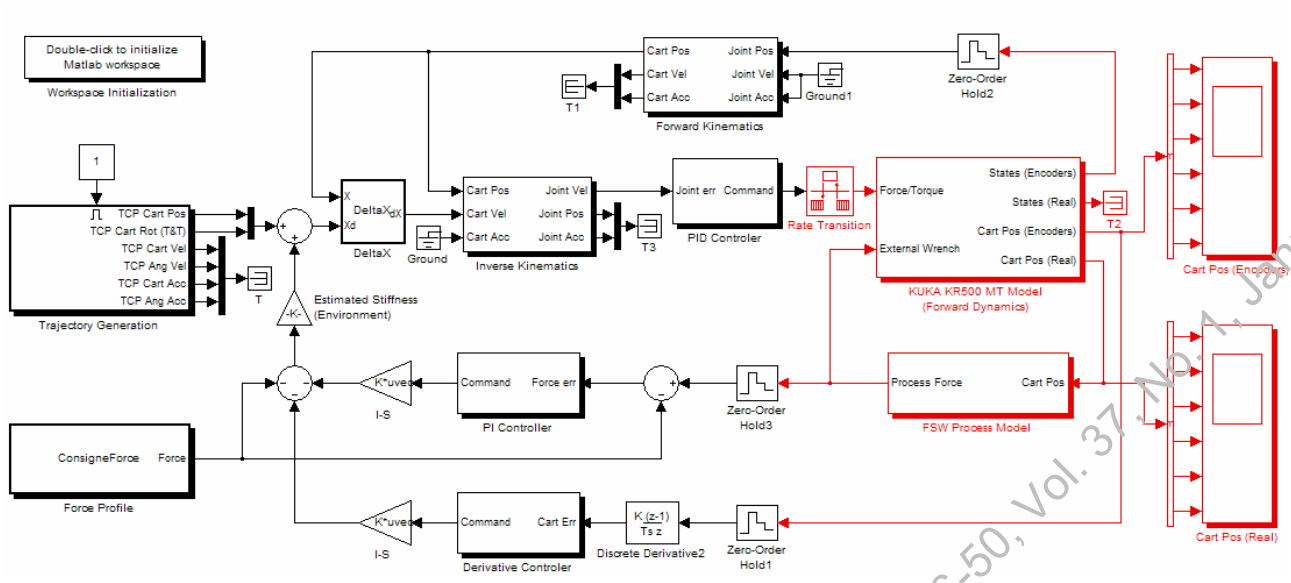

Figure 10 First level view of the MatLAB/Simulink block diagram used to perform multi-rate dynamical simulations of the KUKA KR500 MT performing FSW assembly operations of aerospace components under hybrid external position/force control. The blocks appearing in black, incorporating the trajectory generation and control structure are computed at a 12ms time step (the time step of the KUKA KRC2 control unit). The blocks appearing in red, incorporating the robot forward dynamics and muli-axes FSW process model are computed at a time step ≤1ms. A variable step continuous Dormand-Prince solver (ode45) was used to compute the results of the simulations.

Due to the high stiffness of the process, the computed forces can be of very high amplitude, thereby imposing a time step that was eventually set to a value far less than 1ms, depending of the process parameters and trajectory profile, to provide accurate and stable simulation results.

4.3 Implementation of the force/position control unit

In order to evaluate their performance, the three control structures presented in Subsection 3.2 were implemented in the simulation environment. In all cases, the encoder feedback is integrated using the forward dynamics calculated encoders variables $\boldsymbol{\theta}_E$ while the force sensor readings are emulated using the output of the FSW process model block. All these vector signals are resampled at a 12ms time step using a zero-order hold block. For the 3 candidate control schemes, the first step was the tuning of the gains of the position control loop in order to achieve a motion tracking performance similar to that of the real KR500 MT robot. Secondly, a contact operation with activation of the FSW process model was generated to allow the tuning of the gains of the force feedback loop. Depending on the hybrid force/position control architecture, adjustments also had to be made on the gains of the position control unit, especially with adjustments of the integrator gains in the case of the 2nd control scheme involving superposed position /force control in the tool depth direction.

To illustrate the integration of the control schemes presented in Subsection 3.2, the reader is referred to as the MatLAB/Simulink block diagram appearing in Figure 10 incorporating the external force/position control structure with cascaded control loops in the tool depth direction.

4.4 Initial conditions of the simulation

Due to the fact that no macroscopic model was available for soft or hard real-time simulation of either the entrance or retraction of the tool pin inside/from the FSWelded material, the assumption was made by the authors that the tool plunge and retraction sequences would not be simulated. For that reason, the authors decided to reduce the scope of work to the simulation of the welding sequence, i.e., the progression of the FSW tool in the welded material. According to the authors, such an assumption does not compromise on the ability of the simulation platform to achieve the formulated project objectives in terms of robotized process analysis, design and optimization.

In this context, a proper initial state had to be formulated in order for the robot to stabilize with the tool pin located a few tenths of a millimeter inside the welded material, the different joints being deformed subjected to significant process induced load cases. It was found that the only way of achieving a stable initial robot configuration was to compute compatible encoder and real joint-variables fulfilling the system of coupled differential Eqs. (2.1) in quasi-static regime.

Finally, an efficient strategy identified by the authors to achieve a stable simulation start was to stabilize the tool pin in the material under pure position control at a desired depth command before activating the prescribed linear hybrid force/position control retroaction to reach the required normal force amplitude.

5. Simulations and results analysis

In this section, a performance evaluation of the three hybrid force/position control architectures, as described in Subsection 3.2, is first presented. The second part pertains to the presentation of simulation results in the context of the robotic friction stir lap welding of stringers on a 2024-T3 aircraft component skin followed by a discussion about the observed process-induced phenomena.

5.1 Evaluation of position/force control architectures under change of force set point

Once all implementation work had been completed, the next endeavor of NRC Aerospace research team pertained to the performance evaluation of the three hybrid force/position control architectures presented in Subsection 3.2. In order to achieve this analysis using the MatLAB/Simulink simulation platform, the robot was subjected to a force set point change of 11kN in the starting configuration of the welding sequence as illustrated in Figure 12(a), with the FSW end-effector tool axis pointing downward and tool pin located at coordinate [x, y, z]=[1700mm,-1000mm,500mm]. For the same test case, the force response characteristics of each of the three different hybrid force/position control architectures were obtained and analyzed. The simulated force responses in the FSW tool depth direction obtained with the three linear control schemes are presented in Figure 11.

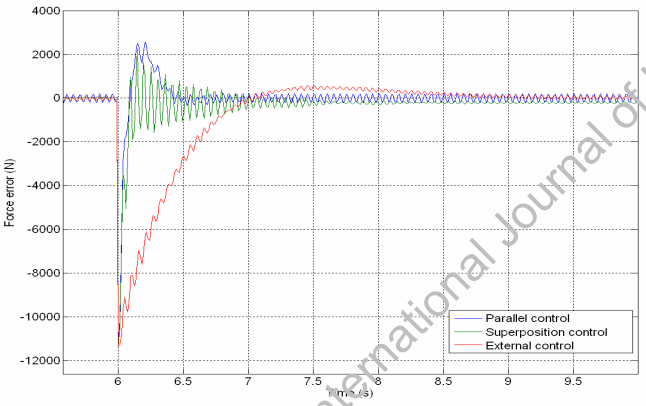

Figure 11 Simulated force response in the FSW tool depth direction to a 11kN force set point change for the 3 hybrid linear force/position control architectures presented in Subsection 3.2, and evaluated using the developed MatLAB/Simulink multi-axis dynamical simulation.

The parallel hybrid force/position control structure with purely force controlled tool depth, as described by Eq. (2.2), exhibits the shortest 5% response time, of approximately 370ms, with an associated negligible residual static error after 500ms. The response shows very little sensitivity to the modeled dynamic perturbation simulating the force variations induced by the tool rotation. On the other hand, this response presents an overange of almost 24% of the nominal force.

The partially decoupled hybrid force/position control structure with superposed control in the tool depth direction, governed by Eq. (2.3), also exhibits a fast response time, of approximately 580ms, with an force response overange of 20%. Its response is characterized by some oscillations induced by the tool rotation that may stem from the intersection of the position and force-controlled subspaces in the tool depth direction. Although these oscillations are rapidly damped, a static error with an amplitude around 200N is raised, illustrating the influence of the integrator gains in the position control feedback loop.

The hybrid external force/position control structure with cascaded control loops in the tool depth direction, governed by Eqs. (2.4) and (2.5), exhibits the poorest response time, with an amplitude around 860ms. It can be explained by the fact that the feedback signal has to be treated through two successive control laws, each being associated with its own response time. However, this response exhibits an interesting overange of only 4.5%, with a static error converging to zero and a good resilience to the oscillation due to the rotation of the tool that are limited to a 50N amplitude.

In the continuation of the study, all simulations were conducted using the hybrid external force/position control structure as this third scheme was chosen for implementation on the NRC Aerospace robotic FSW test-bed (see Figure 2).

5.2 Simulation of robotic friction stir lap welding of stringers on 2024-T3 aircraft component skin

Multiple applications of friction stir welding using the KR500 MT serial industrial robot can be implemented and analyzed using the developed high fidelity dynamical simulation. In order to illustrate the challenges associated to the use of high payload serial industrial robots and the opportunities offered by the new simulation platform, an application of robotic FSW is now presented that is representative of aerospace assembly applications of interest to the authors. The two welding sequences involve friction stir lap welding of stringers on a 2024-T3 aluminum aircraft component skin, involving the complete multi-axial load case as described in Figure 3(b), with, in particular, a 18kN force in the tool depth direction.

The first welding sequence is shown in Figure 12(a). It involves a progression of the tool pin along the stringer of a total 2000mm distance in the +Y direction, with the FSW end-effector tool axis pointing downward and a starting configuration located at coordinate [x, y, z]=[1700mm,-1000mm,500mm]. The second welding sequence, as shown in Figure 13(a), involves a progression of the tool pin along the stringer of a same 2000mm distance in the +Y direction, with a 45° tool axis incidence angle and a starting configuration located at coordinate [x, y, z]=[2000mm,-1000mm,500mm].

These welding sequences were selected to provide insight on the interaction between the industrial robot mechanics, control architecture and heavy process-induced load cases in a large range of robot configurations that are relevant to the planned aerospace assembly applications. As expected, typical issues associated with industrialization of FSW using industrial serial robots can be observed in the simulation results. They are discussed in the following subsections.

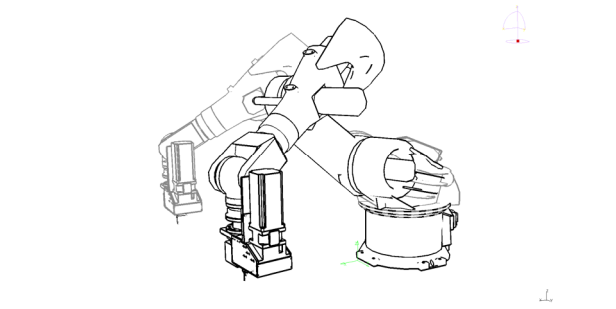

(a)

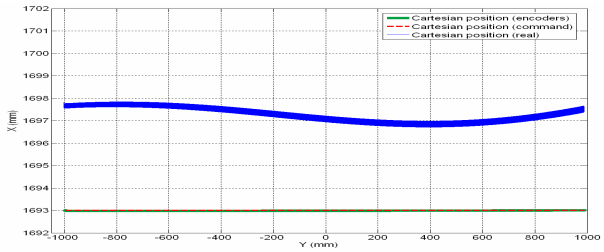

(b)

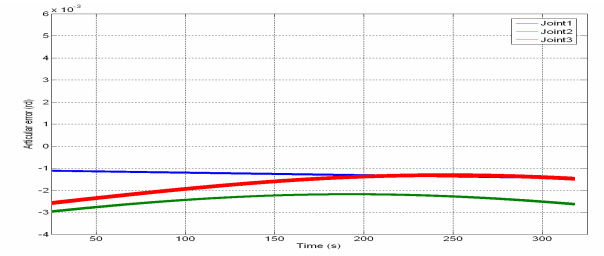

(c)

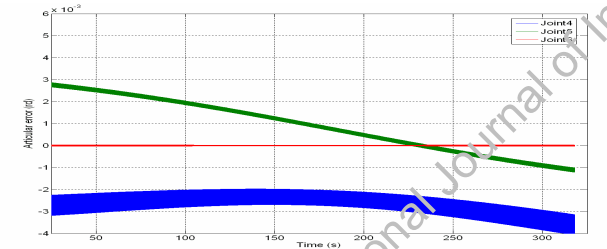

(d)

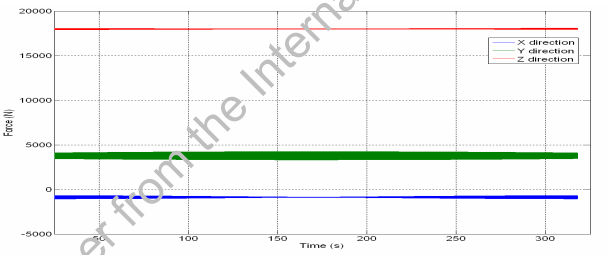

(e)

Figure 12 Results of the simulation of the robotic friction stir lap welding of a stringer on a 2024-T3 aircraft component skin. The welding sequence involves a progression of the tool pin along the stringer of a total 2000mm distance in the +Y direction, with the FSW end-effector tool axis pointing downward and a starting configuration at coordinate [x, y, z]=[1700mm,-1000mm,500mm]. (a) Illustration of the robot postures at the starting (transparent) and final configurations. (b) Simulated tool pin x,y-trajectory. (c) Simulated articular error (difference between encoder readings and real coordinate for joints 1, 2 and 3 and (d) joints 4, 5 and 6. (e) Cartesian forces applied on the FSW tool.

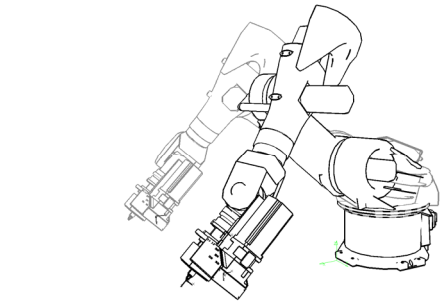

(f)

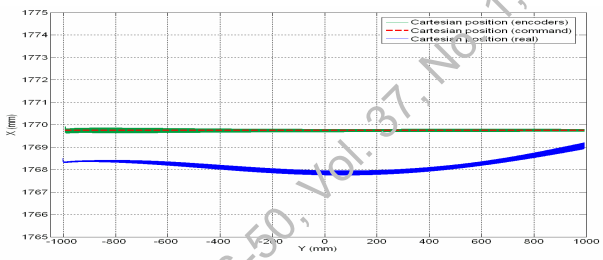

(g)

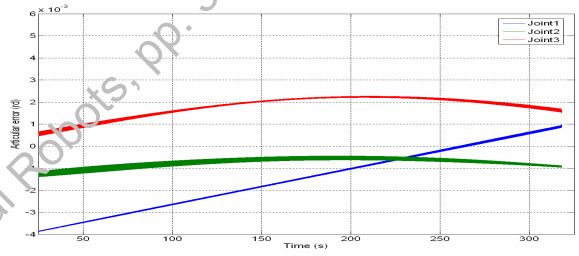

(h)

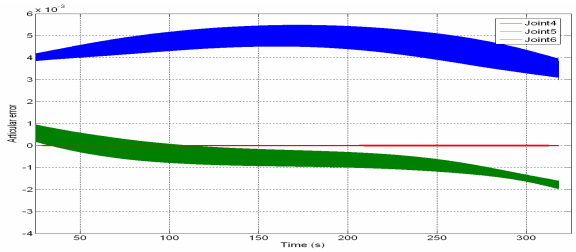

(i)

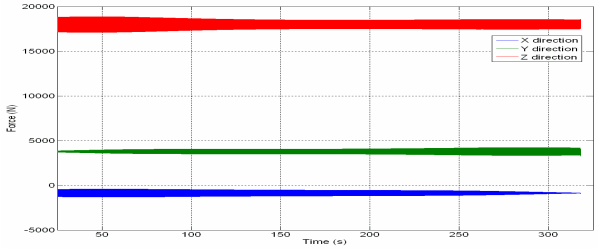

(j)

Figure 13 Results of the simulation of the robotic friction stir lap welding of a stringer on a 2024-T3 aircraft component skin. The welding sequence involves a progression of the tool pin along the stringer of a total 2000mm distance in the +Y direction, with the FSW end-effector presenting a 45° incidence angle and a starting configuration located at coordinate [x, y, z]=[2000mm,-1000mm,500mm]. (f) Illustration of the robot postures at the starting (transparent) and the final configurations. (g) Simulated tool pin x,y-trajectory expressed in the operational frame. (h) Articular error for joints 1, 2 and 3 and (i) joints 4, 5 and 6. (j) Cartesian forces applied on the FSW tool.

5.3 Sensitivity to FSW tool dynamics

During both welding sequences, simulation results appearing in Figs 12(e) and 13(j) show that the industrial serial robot is capable of maintaining the desired constant force level on the welded material, thanks to the force control in the tool depth direction. We notice that the amplitudes of the envelopes of the achieved normal force level vary depending on the robot configurations, with a very low sensitivity to force variations induced by the tool rotation when the FSW end-effector tool axis is pointing downward [Figure 12(e)] but a noticeably larger envelope when the end-effector is used with a 45° incidence angle [Figure 13(j)]. The larger sensitivity of the force feedback loop to the FSW tool dynamics was observed in welding sequences where robot configurations are in the vicinity of singular postures characterized by collinear 4^{th} and 6^{th} joint axes. These observed simulated phenomena provided some valuable guidelines on how to appropriately locate the aerospace component jig in the robot workspace.

Also interestingly, both welding sequences showed well contained oscillations, within aerospace component assembly tolerances, in the achieved tool pin positions, as it can be seen in Figs 12(b) and 13(g). The latter can be explained in small part by the damping in the robot joints and mostly by the effect of the process viscosity that acts as a supplementary physical continuous-time damping factor.

5.4 Lateral FSW tool deviations

As seen in previous subsection, the force control feedback makes the elastic deformations of the robot joints transparent to the process on the tool depth direction. In the welding plane, however, these deformations are not seen by the joint encoders and can freely express depending on the induced load case and solicited robot configurations. In the case of both simulated welding sequences, these lateral tool deviations can be observed by comparing the *real* FSW tool position computed using the robot forward dynamics with the theoretical tool pin trajectory. In the first welding sequence shown in Figure 12(b), lateral tool deviations of up to 5mm amplitude were observed, illustrating the difficulties of the robot to follow the planned trajectory at this level of solicitations. Lateral tool deviations in the case of the second welding sequence can be observed in Figure 13(g). Although the torques on the axes of the spherical wrist are globally low, the induced deformations on the joints are interestingly of the same order of magnitude as those on the three first joints, as depicted in Figs 12(c,d) and 13(h,i), which can be easily explained by the lower stiffness of the wrist joints. In depth analysis of the robot instantaneous kinematics mapping articular errors into Cartesian positional / orientational errors shows, however, that most of the lateral tool deviations stem from deformations of the proximal joints.

The observed process-induced phenomena motivated the authors to synthesize additional feedback control loops to compensate effects of static and dynamic perturbations. The feedback loops were implemented in the MatLAB/Simulink simulation platform for complete certification prior to final integration on the physical test-bed.

6. Conclusion and future investigations

The developed simulation infrastructure allowed the research team to analyze the dynamic interaction between the serial industrial robot mechanics, control architecture and FSW manufacturing process. A performance evaluation of three hybrid force/position control architectures was conducted and simulation results were presented in the context of the robotic friction stir lap welding of 2000mm stringers on a 2024-T3 aircraft component skin with two different FSW tool axis orientation angles. Both simulated welding sequences showed critical process-induced perturbations such as tool oscillations and lateral tool deviations. Recently, the presented simulation platform was used for the validation of advanced real-time feedback control laws for robust handling of critical process-induced perturbations.

Ongoing works of NRC Aerospace research team pertains to the implementation of the aforementioned advanced control feedback loops on the robotic FSW test-bed located at the Aerospace Manufacturing Technology Centre. Other ongoing activities pertain to the detailed design of the robotic FSW system for welding large scale aircraft structural elements, including the development of optimized process parameters involving reduced load cases.

References

[1] , T.W. Nelson, "Friction stir welding-A brief review and perspective for the future", Friction stir welding and processing III, San Francisco, CA, USA, TMS (The Minerals, Metals & Materials Society), Feb. 13-17, 2005, 149-159.

[2] N.G. Tretyak, Paton Welding Journal, Vol. 7 (2002) 10-18.

[3] T. Shinoda, Welding in the World, Vol. 47 (2003) 18-23.

[4] S.W. Kallee, W.M. Thomas, E.D. Nicholas, "Friction stir welding of lightweight materials", Magnesium Alloys and their Applications, Munich, Germany, 26-28 Sept., 2000, 175-190.

[5] S.W. Kallee, W.M. Thomas, E.D. Nicholas, "Application of friction stir welding for aluminium aerospace components", Advanced Aerospace Materials, 19th European Conference of Materials for Aerospace Applications, Munich, Germany, 6-8 Dec., 2000, 33-40.

[6] J.Q. Su, T.W. Nelson, R. Mishra, M. Mahoney, Acta Materialia, Vol. 51 (2003) 713-729.

[7] M.A. Sutton, B. Yang, A.P. Reynolds, R. Taylor, Materials Science and Engineering A, Vol. 323 (2002) 160-166.

[8] S.R. Sharma, R.S. Mishra, J.A. Baumann, R.J. Lederich, R. Talwar, "Microstructural characterization of a FSW 7050 Al alloy", Friction Stir Welding and Processing II, San Diego, CA, USA, TMS (The Minerals, Metals & Materials Society), 2-6 March, 2003, 209-217.

[9] R.V. Preston, H.R. Shercliff, P.J. Withers, C. Smith, Acta Materialia, Vol. 52 (2004) 4973-4983.

[10] P.A. Colegrove, H.R. Shercliff, Science and Technology of Welding and Joining, Vol. 8 (2003) 360-368.

[11] L. Cederqvist, A.P. Reynolds, Welding Journal, Vol. 80 (2001) 281-287.

[12] J. Arbegast, "Using process forces as a statistical process control tool for friction stir welds", Friction stir welding and processing III, San Francisco, CA, USA, TMS (The Minerals, Metals & Materials Society), Feb. 13-17, 2005, 193-204.

[13] D. Bolser, R. Lederich, R. Talwar, J. Baumann, Welding in the World, Vol. 48 (2004) 255-259.

[14] M.J. Brooker, D. van, S.W. Kallee, P.D. Sketchley, "Applying friction stir welding to the Ariane 5 (space launch vehicle) main motor thrust frame", 2nd International Symposium of Friction Stir Welding, Gothenburg, Sweden, Abington, 26-28 June, 2000.

[15] R. Talwar, D. Bolser, R.J. Lederich, J. Baumann, "Friction stir welding of airframe structures", 2nd International Symposium of Friction Stir Welding, Gothenburg, Sweden, Abington, 26-28 June, 2000.G. W.

[16] M. Skinner, R.L. Edwards, “Improvements to the FSW Process using the Self-Reacting Technology”, Materials Science Forum Vols. 426-432 (2003) pp. 2849-2854.
[17] G. Voellner, O. Kellenberger, D. Lohwasser, and J. Silvanus. “3-Dimensional Friction Stir Welding using a Modified High Payload Robot,” 6th International Friction Stir Welding Symposium, Saint Sauveur, Canada, 10-13 October 2006.
[18] L. Dubourg, F.- O. Gagnon, F. Nadeau, L. St-Georges, M. Jahazi, “Process window optimization for FSW of thin and thick sheet Al alloys using statistical methods”, 6th International Friction Stir Welding Symposium, Saint Sauveur, Canada, 10-13 October 2006.
[19] H.Takahara, Y. Motoyama, M.Tsujikawa, S.Oki, S.W. Chung, andK.Higashi, “Allowance of Deviation and Gap in Butt Joint on Friction Stir Welding”, Advanced Materials Research Vols. 15-17 (2007) pp 375-380.
[20] Angeles, J., Fundamental of Robotic Mechanical Systems: Theory, Methods and Algorithms, Springer, New York, second edition
[21] W. Khalil, E. Dombre, “Modélisation identification et commande des robots”, Hermes Science Publications, Paris, 1988, 1999, second edition
[22] “Using Simulink, version 5” The MathWorks, Inc, April 2003, sixth edition.
[23] Dracup BJ, Arbegast WJ. “Friction stir welding as a rivet replacement technology.” In: Proceedings of the 1999 SAE aerospace automated fastening conference & exposition, Memphis, October 5–7, 1999.
[24] Christner B, McCoury J. “Development and testing of friction stir welding (FSW) as a joining method for primary aircraft structure.” In: Fourth international FSW symposium, Park City, Utah, May 14–16, 2003.
[25] V. Strombeck, C. Shilling, and J. F. D. Santos. “Robotic friction stir welding – tool, technology and applications,” 2nd International Friction Stir Welding Symposium, Gothenburg, Sweden, 2000.
[26] M. Soron, I. Kalaykov. “A Robot Prototype for Friction Stir Welding,” IEEE Conference on Robotics, Automation and Mechatronics, Bangkok, Thaïlande, Dec. 2006.
[27] C. Smith, J. Hinrichs, “Development and Qualification of a Production Capable FSW Process for 25 mm Deep Robotic Friction Stir Welds,” In: Proceedings of the 6th Int. Friction Stir Welding Symposium, St. Saveur, Quebec, October 2006.
[28] G. Duelen and K. Schröer, “Robot calibration: Method and results,” Robot. Computer-Integrated Manufact., vol. 8, no. 4, pp. 223–231, 1991.
[29] K. Schröer, “Theory of kinematic modeling and numerical procedures for robot calibration,” Robot Calibration, H. R. Bernhardt and S. Albright, Eds. London, England: Chapman and Hall, 1993, pp. 157–196.
[30] J. Denavit and R.S Hartenberg, “A kinematic notation for lower –pair mechanisms based on matrices,” ASME J. Applied Mechanics, 77, pp. 215–221, 1955.
[31] L. Dubourg, A. Merati, M. Jahazi, “Manufacturing of aircraft panels by friction stir lap welding of 7075-T6 stringers on 2024-T3 skin: Part I. Process optimization”, submitted to the 7th International Friction Stir Welding Symposium, Kobe, Japan, 20-22 May, 2008.
[32] Crawford, R., Cook, G.E., Strauss, A.M., and Hartman, D.A. “Modeling of friction stir welding for robotic implementation,” Int. J. Modeling, Identification and Control, Vol. 1, No. 2, pp.101–106, 2006.
[33] Xi. Zhao, P. Kalya, R. G. Landers, and K. Krishnamurthy “Design and Implementation of a Nonlinear Axial Force Controller for Friction Stir Welding Processes,” In: Proceedings of the 2007 American Control Conference, New York City, USA, July 11-13, 2007.
[34] “SimMechanics™ 2 User’s Guide” The MathWorks, Inc, 2001-2008.